EVALUATION OF GEOGRID PULLOUT BEHAVIOR IN CLAYEY SAND USING SMALL-SCALE TESTS

S. H. C. Teixeira
GeoHydroTech - Brazil

B. S. Bueno
EESC - University of Sao Paulo - Brazil

ABSTRACT: The knowledge of interaction mechanisms between soil and geosynthetics is fundamental for designing soil-reinforced structures. However, because of the variety of surface geometry found in commercially available geosynthetics, the interaction between soil and inclusions can be of different types. For the geogrids, the pullout interaction mechanism is the one that, in many cases, best represents the field situations. The paper presents a brief discussion about the pullout mechanism of geogrids. It is also presented a numerical model that can be used to evaluate the behaviour of geogrids, with any length, using results from small-scale pullout tests and from non-confined tensile tests. The results from tests performed using a large-scale device and numerical simulations, using data from small-scale tests, are compared in order to show the viability of using small-scale pullout tests of geogrids buried into fine soils. A discussion about analyses of applied normal stress and embedded length on the interaction mechanism between soil and inclusion is also presented.

1 INTRODUCTION

In reinforced soil structures, such as earth retaining walls, steep slopes and embankments on soft soils, the behaviour of the system is controlled mainly by the shear strength of the soil and by the mechanical properties of the reinforcement. The main function of the inclusions is to redistribute internal stresses within the soil mass in order to enhance the stability of the reinforced structure. To behave properly, the inclusions should undergo tensile strains, transferring loads from the unstable portions of the soil mass to the stable areas, creating, therefore, a more stable soil mass.

The redistribution of internal stresses within the reinforced soil mass and the deformation response of the structure depend on the shear strength of the soil, tensile strength of the inclusions and stress transfer mechanisms that take place between soil and inclusions. The understanding of the soil-reinforcement interaction is important since it provides insight into overall behaviour of reinforced soil structures.

This paper presents theoretical and experimental studies about the pullout phenomena. The applied normal stress and the embedded length were evaluated. The studies were carried out using a large dimension pullout test device, with technical characteristics similar to many others found in international literature, and a small dimension apparatus.

The results obtained from pullout tests in a small box were treated with a numerical model in order to allow anticipate the pullout behaviour of large dimension samples of geogrid.

2 PULLOUT MECHANISM OVERVIEW

The interaction mechanism between soil and geogrid is more complex than the one that occurs between soil and strips or sheets. The pullout resistance of geogrids has two components: a) interface shear resistance and b) soil passive resistance on transversal ribs. The interface shear resistance can also be separated into friction and adhesion components. The relations between interface and passive resistances on the total pullout resistance depend on the geogrid geometry, soil grain size and soil compaction.

2.1 *Interface shear resistance mechanism*

The frictional component of the pullout resistance along the interface between granular soils and geogrid reinforcements can be defined as (Jewell *at al.,* 1984):

$$P_f = 2 \cdot A_a \cdot \sigma_n \cdot \alpha_s \cdot tg\delta \quad (1)$$

where: A_a is the total anchored area of geogrid; σ_n is the normal stress acting on the inclusion; α_s is the fraction of the solid area in relation to the total area of geogrid and δ is the interface friction angle.

Cohesive soils, on the other hand, can supply an additional pullout resistance due to adhesion of their particles to the geogrid surface. The Equation (1) can be rewritten to consider the adhesion, α, between soil and geogrid.

$$P = 2 \cdot A_a \cdot \alpha_s \cdot (\sigma_n \cdot tg\delta + \alpha) \quad (2)$$

The shear resistance on interface between longitudinal elements and granular soils is highly affected by soil density and confinement. Under high confinement, most soils show a contractile behaviour when sheared. On the other hand, under low confinement, most compacted soils show a dilatant behaviour when sheared. The Figure 1 illustrates the saw tooth model for soil dilatancy (Houlsby, 1991), where horizontal displacements impose to the system an increase in height, δ_v. An additional energy is required for the system in order to cause a vertical shear displacement. This energy is numerically equal to the work:

$$W_n = \sigma_n \cdot A \cdot \delta_v \quad (3)$$

where A is the cross sectional area of the sheared soil element.

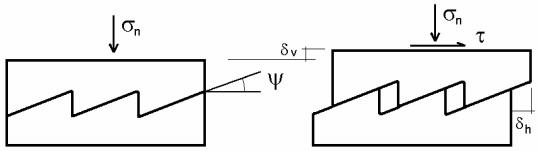

Figure 1- Saw tooth model for dilatancy (Houlsby, 1991).

When longitudinal ribs of geogrids are buried in a dense soil mass, under moderate confinement stresses and moving subjected to a pullout force; the soil tends to dilate. On this situation, if the surrounding soil is prevented to dilate, the confinement stress increases. The magnitude of this increment depends on soil density, grain size distribution and initial confinement, and if the system is considered to be non-dissipative, it is proportional to the work W_n. The result of the inhibited dilatancy is, therefore, an increasing in the frictional shear resistance.

2.2 *Passive resistance mechanism*

The evaluation of the passive resistance, given by the soil while the geogrid transversal ribs are pulled out, is more complex than the evaluation for interface shear strength. However, it can be done considering the transversal elements of geogrids as several shallow foundation members laying transversal to the pullout direction (Bergado *et. al.*, 1994). The passive resistance depends, therefore, on the geogrid geometry and type of soil.

Two mechanism of bearing capacity are usually adopted to estimate the maximum pullout resistance, they are called general failure and punching failure mechanisms. They provide an upper and a lower bound limits to the pullout test results.

The passive resistance equation for the first mechanism is based on Terzaghi–Buisman bearing capacity equation; for the second mechanism; the equation is based on punching failure mode of deep foundations. The passive resistance (T_f) for the first mechanism is given by (Jewell *et. al.*, 1984):

$$T_f = (c \cdot N_c + \sigma'_n \cdot N_q) \cdot N \cdot W \cdot D \tag{4}$$

where N, W and D are the number, the length and the diameter of geogrid transversal elements, c is the soil cohesion, σ'_n is the vertical normal stress and

$$N_q = e^{\pi \cdot \tan\phi} \cdot \tan^2\left(45 + \frac{\phi}{2}\right) \tag{5}$$

$$N_c = \left(N_q - 1\right) \cdot \cot\phi \tag{6}$$

where ϕ is the internal friction angle of soil.

This equation provides an upper limit to passive resistance of soils reinforced with geogrids (Palmeira & Milligan, 1989b; Jewell, 1990 e Shivashankar, 1991). The equation used to calculate the resistance by punching is similar to Equation (4), but the variables N_q and N_c are replaced by:

$$N_{q1} = e^{\left(\frac{\pi}{2}+\phi\right)\tan\phi} \cdot \tan\left(45 + \frac{\phi}{2}\right) \tag{7}$$

$$N_{c1} = \left(N_{q1} - 1\right) \cdot \cot\phi \tag{8}$$

The punching failure equation provides a lower limit to the pullout resistance of geogrids (Palmeira & Milligan, 1989a). Most of passive resistance experimental values found on the literature represent an intermediary situation between these two boundaries.

3 TEST EQUIPMENT

3.1 *Large-scale pullout test device*

The pullout test device used on this work was described by Teixeira & Bueno (1999), and consists of a rigid structure, with rectangular transversal section made of steel plates, reinforced with U steel beams, as showed in Figure 2. A steel frame supports an electric system used to apply the pullout load. This system is capable of applying up to 60 kN of tensile force in a geosynthetic sample.

The device uses an air bag to apply uniform surcharges and to simulate confinement conditions representative of field conditions. The air bag is connected through a plastic hose to a manometer that indicates the pressure inside the air bag.

The data measured during testing include: a) pullout force, using a load cell coupled to the clamp; b) normal stresses on soil mass, using two total stress cells buried in the soil mass at about 10 mm over the geogrid; and c) displacements, using six displacement transducers that were connected by inextensible wires along the geogrid specimen. One manometer was also used to measure the air pressure inside the inflatable bag.

The soil is compacted on test box in layers of 75 mm to provide adequate compaction. Tamping is carried out with a manual hammer that has a circular base of 120 mm in diameter, weighting 60 N, and falling from a height of 300 mm. The soil is compacted in six layers, three under and three above the geogrid.

The inextensible tell-tail wires used for displacement measurement along the reinforcement are connected to six displacement transducers placed on the rear end table. The wires are encased in a polyethylene tube placed along the reinforcement. The two total stress cells are positioned over a 10 mm layer of soil at different positions along and above the reinforcement sample. All tests are conducted at displacement rate of 4.6 mm/min.

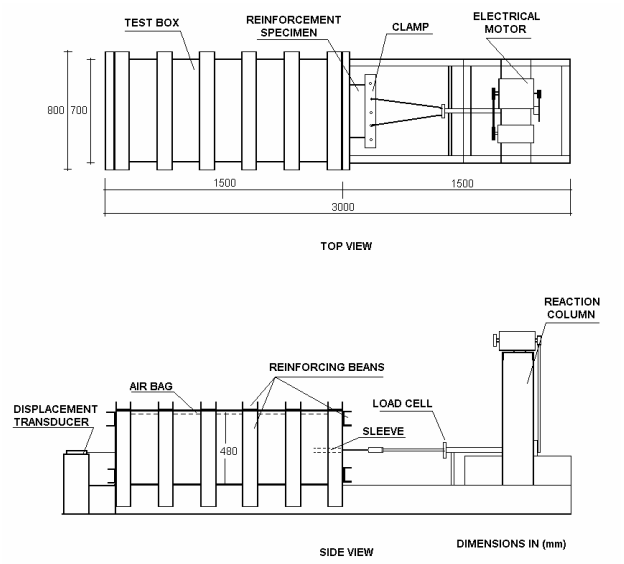

Figure 2- Schematic view of pullout test apparatus (Teixeira & Bueno, 1999).

3.2 *Small pullout test device*

The small pullout test device is composed by a pullout box, a surcharge application system, a tensile testing machine and instrumentation. The box is made of steel plates rein-

forced with square section tube, as shown in Figure 3. The surcharge system consists of an air bag, positioned between the soil and the box cover, a manometer and an air-compressor. A pore-pressure transducer, PPT, a total stress cell, TSC, and a load cell compose the instrumentation of this equipment. A data acquisition system, connected to a computer, is used for measure the displacements and pullout force during the test.

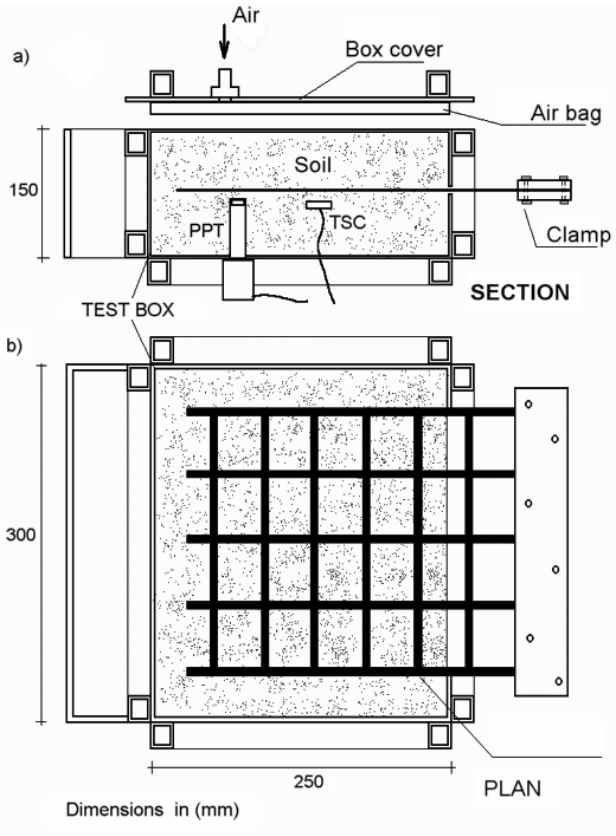

Figure 3 – Schematic of small pullout test box: a) Section, b) Plan.

In this device, the soil is allowed to expand during testing, since the soil surfaces are covered with flexible air bags. In order to minimise side friction during pullout testing, the walls of the boxes are internally covered with two lubricated polyethylene membranes.

The small-scale pullout test is carried out on the pullout box showed on Figure 3, using a 230 mm long and 265 mm wide piece of geogrid. That box is attached to the base of a tensile testing machine and the geogrid is attached to a clamp. A curve that relates pullout force and imposed displacement, δ, can be obtained from this test.

The load vs. displacement curves, obtained from small tests, provide important qualitative information. However, the collected data can be incorporated into a numerical model in order to predict results obtained using large dimension pullout boxes.

Table 1- Properties of tested soils

Properties	Values
Maximum dry unit weight, γ (kN/m^3)	18.85
Optimum water content, w_{op} (%)	10.2
Angle of internal friction, ϕ (°)	36
Cohesion, c (kPa)	15
Degree of compaction (%)	100
Classification on Unified System	SM-SP

4 MATERIALS

4.1 *Soil*

A clayey sand soil was used on both types of pullout tests. The grain size distribution curve of is presented on Figure 4, and other properties are listed on Table 1. The optimum compaction parameters and degree of compaction are related to Standard Proctor energy. The strength parameters of the soil were determined in direct shear tests with the soil compacted with degree of compaction indicated on Table 1.

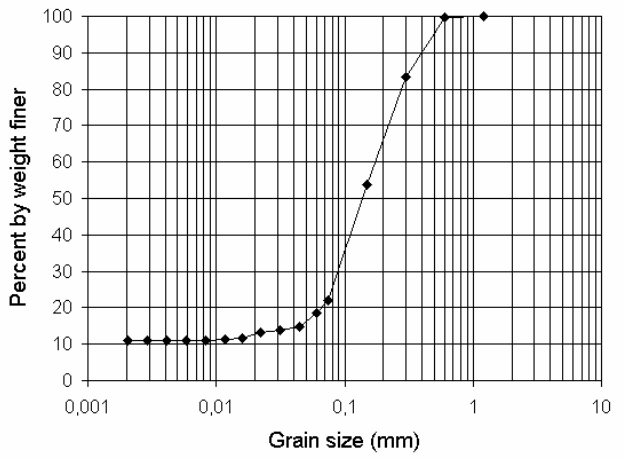

Figure 4 – Grains size distribution curves of soils used on pullout tests.

4.2 *Geogrid*

The used geogrid consists on a uniaxial polyester grid coated with PVC. The geogrid has a square mesh with an opening of 29 x 28 mm. The width of longitudinal ribs is 8 mm and of transversal ribs is 3 mm. The thickness of transversal ribs is 1.5 mm. The fraction of the solid area in relation to the total area of this geogrid, α_s, is, therefore, 0.29. Figure 5 presents the curve force vs. strain of the geogrid.

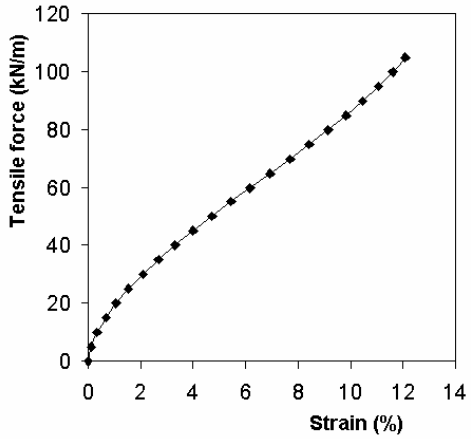

Figure 5 – Tensile force vs. strain curve for the used geogrid.

5 TESTS

5.1 *Testing program*

Large and small-scale pullout tests were performed to estimate the pullout interaction between soil and geogrid and evaluate the feasibility of using small boxes for evaluate the pullout resistance of geogrids in fine-grained soils. Three different normal pressures and three different geogrid lengths were considered on tests. Table 2 presents the testing program for both types of pullout test.

Table 2- Program of large and small-scale pullout tests.

Test	Surcharge (kPa)	Length (mm)	Type of test
LS1	25	350	Large-scale
LS2	25	600	Large-scale
LS3	25	1200	Large-scale
LS4	50	600	Large-scale
LS5	100	600	Large-scale
SS1	25	600	Small-scale
SS2	25	600	Small-scale
SS3	25	600	Small-scale

5.2 *Large-scale pullout test results*

A typical pullout test result on a long geogrid specimen is presented in Figure 6, where the total applied pullout force vs. displacement on each measuring node is plotted. The locations of nodes whose displacement were measured by displacement transducers, DT, are presented at the legend.

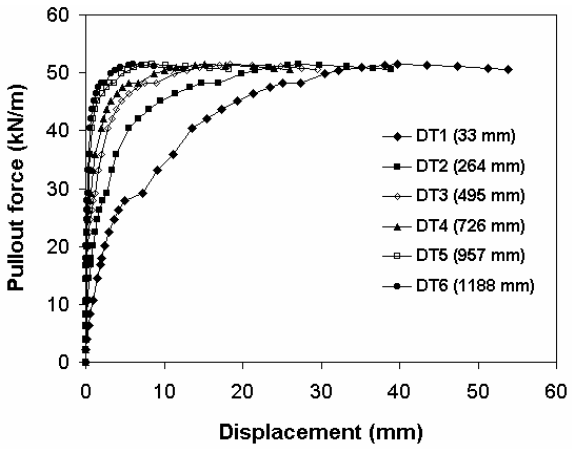

Figure 6- Force vs. displacement curves for the test LS3.

The effect of geogrid length on pullout load is evaluated though the tests LS1, LS2 and LS3 and the results are shown on Figure 9. It can be noted that the increasing in length is followed by increasing on maximum pullout force, stiffness modulus and frontal displacements at peak.

5.3 *Small-scale pullout test results*

The small-scale pullout tests were performed using the same geogrid and similar test conditions to those of large-scale pullout test. Figure 8 presents the results of tests described in Table 2. The presented values of pullout stress are obtained by dividing the pullout force by the total geogrid area. The pullout stress is defined as:

$$\tau = \frac{F_{ar}}{2b.(l-\delta)} \tag{9}$$

where F_{ar} is the pullout force referring to the displacement δ, b is the width of geogrid specimen and l the initial embedded length of specimen.

The pairs of experimental values τ x δ fit well to the following exponential function:

$$\tau = \tau_{ult}\left(1 - e^{\frac{-k_i \cdot \delta}{\tau_{ult}}}\right) \tag{10}$$

where τ_{ult} is the maximum values of τ for the exponential function and k_i is the initial tangent of the τ x δ curve.

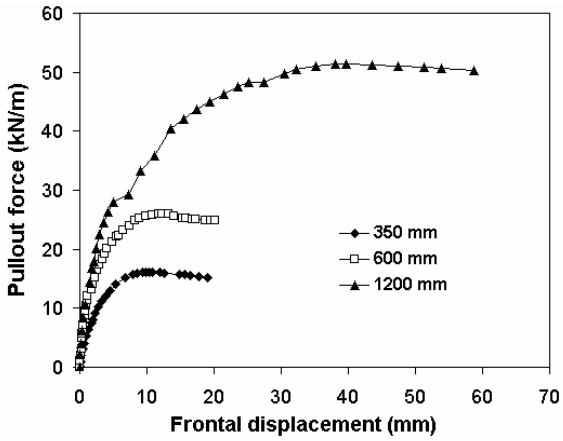

Figure 7- Results of tests on different geogrid length.

Besides the pairs of values τ x δ, Figure 8 also presents the fittings for the experimental values using the exponential function introduced by Equation 10

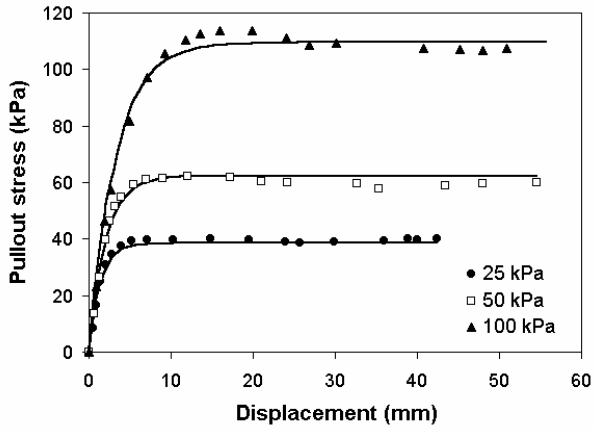

Figure 8- Results of small-scale pullout tests.

The maximum values of pullout stress, presented in Figure 8, can be plotted against the normal stress in order to determine the equivalent adhesion and friction angle between soil and geogrid, Figure 9. Based on this procedure, it is possible to determine the pullout failure envelope.

$$\tau_{ult} = 8 + \sigma \cdot tg25° \tag{11}$$

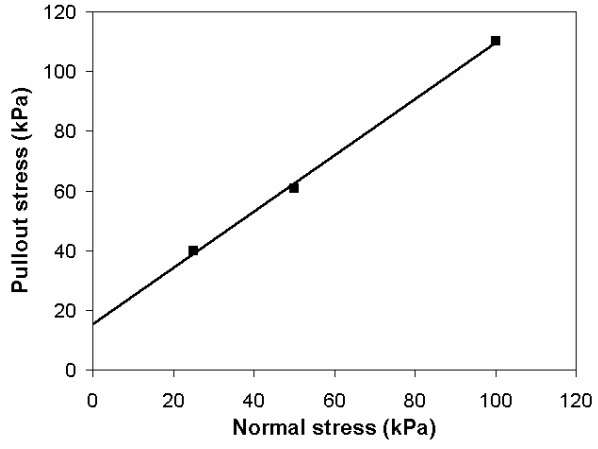

Figure 9- Pullout failure envelope.

In a similar way, the initial tangents to the τ x δ curves can be correlated with the correspondent normal stresses using the following expression:

$$k_i = m \cdot \gamma_w \cdot \left(\frac{\sigma}{P_{atm}} \right)^n \quad (12)$$

where *m* and *n* are parameters to be determinate, γ_w is the specific weight of water and P_{atm} is the atmospheric pressure. The determination of parameters m and n can be made by plotting the values of ln(k_i) against the values of ln(σ/P_{atm}). The points are fitted with a linear function. The parameter *n* corresponds to the tangent of the linear function and *m* can be determinate by:

$$m = \frac{e^a}{\gamma_w} \quad (13)$$

where *a* is the interception of the linear function with ln(σ/P_{atm}) axis.

The obtained parameter values for the performed tests were m= 1656 and n= 0.1328. Therefore, the function that relates the initial tangent to the τ x δ curves with the normal stress is:

$$k_i = 1656 \cdot \gamma_w \cdot \left(\frac{\sigma}{P_{atm}} \right)^{0.1328} \quad (14)$$

Using Equations (10), (11) and (14), it is possible to plot the τ x δ curve for any normal stress between the tested limits. It was shown in Figure 8 that the exponential function fitted pretty well to the experimental data for the tested normal stresses. Therefore, the presented formulation is able to predict the pullout stress for any combination of normal stress and geogrid displacement, considering the tested situation.

6 PREDICTION OF LARGE-SCALE PULLOUT BEHAVIOR FROM SMALL-SCALE TESTS

6.1 *Model for small pullout tests*

A model was developed to predict large-scale pullout test results of extensible geogrids using small-scale pullout test results and load vs. strain curve from unconfined tensile test of the geogrid. The model is capable of predicting displacement, strain and load transfer profiles along the entire geogrid length, as well as the load vs. displacement curve in any point along the geogrid.

The input in formulation includes:

Tensile force vs. strain curve obtained from unconfined tensile test on a geogrid specimen, Figure 5,

Pullout stress vs. displacement curve obtained from small-scale pullout test, as shown in Figure 8.

As showed in Figure 10, the geogrid is modelled as a sequence of segments. There are two displacements, $\delta_{i,j}$ and $\delta_{i,j+1}$, associated to each segment, where *i* is the interaction number and *j* is the segment number. The displacement at the end of each segment is equal to the displacement at the beginning of following segment.

The frontal force, $F_{1,1}$, must be initially assumed in the first interaction, and should be dissipated along the geogrid length. The residual value, $F_{1,n+1}$, is calculated at the final node of the last segment. If the residual value is higher than zero, subsequent lower value for $F_{1,1}$, is assumed in the next interaction. Otherwise, if the residual value is lower than zero, the value is increased until the residual force in last segment tends to zero.

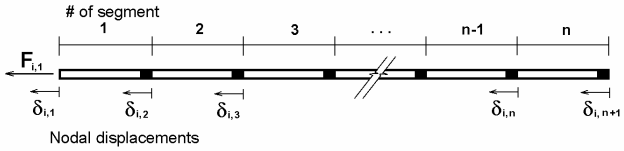

Figure 10- Definition of geogrid on model.

The steps involved in this procedure are summarised as follows:

1- Assume a small initial displacement, $\delta_{1,1}$;

2- Obtain an initial pullout load, $F_{1,1}$, that corresponds to the displacement $\delta_{1,1}$. A first approach involves considering that the geogrid is rigid and the applied frontal displacement occurs along its entire length;

3- Compute the pullout resistance, $R_{1,1}$, for the first segment of geogrid, using the displacement $\delta_{1,1}$ and the τ x δ curve from small-scale pullout test;

4- Compute the average strain, $\varepsilon_{1,1}$, on segment 1, using the curve that relates pullout stress with strain and considering that $(F_{1,1} - R_{1,1}/2)$ is acting in entire segment;

5- Compute the displacement $\delta_{1,2}$, using the equation:

$$\delta_{1,2} = \delta_{1,1} - \varepsilon_{1,1} \cdot L \quad (15)$$

where *L* is the length of the segment.

7- Calculate the force, $F_{1,2}$, acting in the second segment, as follows:

$$F_{1,2} = F_{1,1} - R_{1,1} \quad (16)$$

8- Using the new pair of force and nodal displacement values, $\delta_{1,2}$ e $F_{1,2}$, repeat the steps (2) – (6) to obtain the force and nodal displacement values of the third segment. Repeat this process *n+1* times until the pair of values $\delta_{1,n+1}$ e $F_{1,n+1}$, corresponding to the end of the geogrid is obtained.

9- If the value of $F_{1,1}$ is correct, the value of $F_{1,n+1}$ will be zero. Otherwise, the interactive continues and a new value for the applied force value must be assumed until the value of $F_{i,n+1}$ approaches to zero. The following expression was found useful to estimate the assumed force $F_{i,1}$:

$$F_{i,1} = F_{i-1,1} - \frac{F_{i-1,n+1}}{k} \quad (17)$$

where k is constant with values laying between 5 and 20. Higher k values facilitate convergence of the interactive process, but result in a larger number of interactions.

This procedure is repeated for several frontal displacements until that a series of $\delta_{i,1}$ and $F_{i,1}$ values are obtained, in order to plot the computed displacement vs. frontal load curve. Data obtained during the process can also be used to plot other load profiles along the geogrid length during any simulation phase.

6.2 *Prediction*

Considering the data obtained from small-scale pullout tests, Figure 8, as well the result from the geogrid tensile test, Figure 5, it is possible to simulate the large-scale pullout test results using the presented numerical model. Figure 11 presents a comparison between experimental results form large dimension pullout test and predicted results.

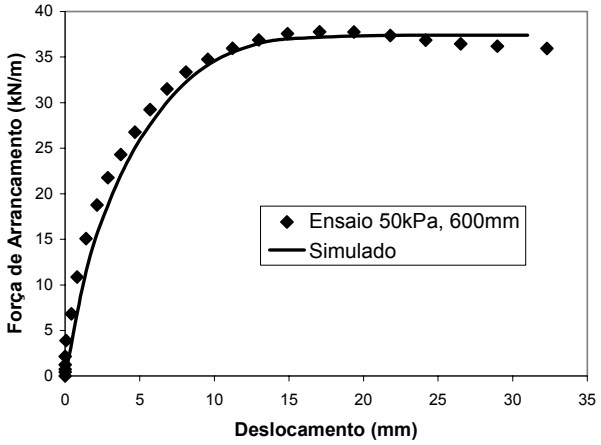

Figure 11- Comparison between LS4 pullout test and simulation results.

The maximum pullout force values for the five large-scale pullout tests and their equivalent simulation results are presented on Table 3. The simulation results are also compared with that obtained from large-scale tests in terms of percentage. As can be noticed from Figure 11 and Table 3, the simulation results are similar to experimental values obtained from large-scale test. The differences between two processes are small except for test LS5 that showed a variation higher than 20%.

A possible explanation for the difference in results is because the buried geogrid did not behave as a rigid body during tests under high normal stresses, considering that one of the premises of the analytical model is the knowledge of geogrid length inside the soil during small-scale tests. It is possible that the specimen length changes during the test due the material strain under pullout effort. This was not considered during the pullout stress determination and the variation of embedded length should be considered.

Table 3- Large-scale tests and simulation results.

Test	Surcharge (kPa)	l (mm)	Pullout force (kN/m)		ΔF (%)
			Tested	Simulated	
LS1	25	350	14.0	13.5	-3.6
LS2	25	600	24.9	23.2	-6.8
LS3	25	1200	49.9	46.4	-7.0
LS4	50	600	36.2	37.4	+3.3
LS5	100	600	53.7	65.7	+22.3

7 CONCLUSIONS

The feasibility of using a numerical model with small-scale pullout test results for evaluate the pullout behaviour of geogrids with any length and embedded in clayey sand was investigated on this study. From the obtained results, some relevant conclusions can be reached:

Although large-scale and field tests are considered the best ways to carry out pullout tests, the few presented results suggest the possibility of using small-scale pullout tests to evaluate the geogrid pullout behaviour, when the grid is embedded by fine grained soils. Due the few experience with this type of test, a carefully interpretation of its results must be exercised.

The small-scale pullout test results can be conveniently interpolated for non-tested normal stresses, aided by analytical modelling. For the tested conditions, it was noticed that the pullout strength has a linear relation with the applied normal stress.

The presented numerical model can be used for evaluating the pullout behaviour of any-length extensible geogrid if small-scale pullout test results are available.

Some important parameters such as geogrid geometry, length and extensibility, type of soil are already considered on input data of the model.

ACKNOWLEDGEMENTS

The authors would like to express their thanks to FAPESP (Foundation for Research Supporting of Sao Paulo State) for the financial supporting that made this work possible.

8 REFERENCE

BERGADO, D. T., CHAI, J. C., ALFARO, M. C., & BALASUBRAMANIAM, A. S., 1994: Improvement Techniques of Soft Ground in Subsiding and Lowland Environment, A. A. Balkema, Rotterdam, Netherlands.

JEWELL, R. A., 1990: Reinforcement Bond Capacity, Geotechnique 40(3), pp. 513 – 518.

JEWELL, R. A., MILLIGAN, G. W. E., SARSBY, R. W. & DUBOIS, D., 1984: Interaction Between Soil and Geogrids, Proceeding of the Symposium on Polymer Grid Reinforcement in Civil Engineering, Science and Engineering Research Council and Netlon Limited, pp. 18 – 30.

PALMEIRA, E.M. & MILLIGAN, G.W.E., 1989a: Large Scale Direct Shear Tests on Reinforced Soil, Soil and Foundations, 29(1), pp. 18 – 30.

PALMEIRA, E.M. & MILLIGAN, G.W.E., 1989b: Scale and Other Factors Affecting the Results of the Pullout Tests of Grids Buried in Sand, Geotechnique 39(3), pp. 551 – 584.

SHIVASHANKAR, R., 1991: Behaviour of Mechanically Stabilised Earth (MSE) Embankment and Wall System With Poor Quality Backfills on Soft Clay Deposits Including a Study of Pullout Resistances, Doctoral Dissertation Submitted, Asian Institute of Technology, Bangkok.

TEIXEIRA, S.H.C & BUENO, B.S., 1999: Um Equipamento para Ensaios de Arrancamento em Geossintéticos Geossintéticos' 99, Rio de Janeiro, pp. 215 – 222 (in Portuguese).